SEISMIC HAZARD ANALYSIS FOR THE TDC2/TCC2 FACILITY AT CERN: A MULTIVARIATE GEOSTATISTICAL APPROACH

E. Alakbarli[1], M. Andreini[2], Y. Kadi[3], S. La Mendola[4], A. Libertà[5] & M. Guarascio[6]

[1] University of Rome "La Sapienza", Rome, Italy, emin.alakbarli@uniroma1.it

[2] CERN – European Organization for Nuclear Research, Meyrin, Switzerland, marco.andreini@cern.ch

[3] CERN – European Organization for Nuclear Research, Meyrin, Switzerland, yacine.kadi@cern.ch

[4] CERN – European Organization for Nuclear Research, Meyrin, Switzerland, saverio.la.mendola@cern.ch

[5] University of Rome "La Sapienza", Rome, Italy, angelo.liberta@uniroma1.it

[6] University of Rome "La Sapienza", Rome, Italy, massimo.guarascio@uniroma1.it

Abstract: *A comprehensive seismic hazard analysis was performed at CERN to assess the potential of earthquake-induced ground motions and their impact on the site's structures and facilities. This study focuses on the underground facilities TCC2 and TDC2, critical components of the Super Proton Synchrotron (SPS) complex. Accurate seismic hazard analysis is relevant for the overall risk assessment, also ensuring the operation of SPS. Seismic data from recording stations located in Switzerland, France, and Italy were collected within a 150-km radius area centred in the TCC2. The collected raw data were then filtered to obtain specific frequency ranges of interest, enabling efficient processing and analysis for accurate seismic hazard analysis of the TCC2 and TDC2. This research proposes an innovative model, synthesising old ideas and insights from the team led by the senior author of the present paper, Massimo Guarascio, that integrates multivariate statistical analysis methodologies with geostatistical ones, addressing three critical aspects of seismic modelling: directional anisotropy of the value and the arrival time of the Peak Ground Acceleration (PGA), geographical continuity in terms of space correlation function describing the apparently irregular variations between data pairs. The experimental validation of a geostatistical estimator accuracy is carried on checking the estimation errors in all the location points of the recording stations. In these points, the recorded values and estimated ones are both known. This model allows a more complete seismic assessment of critical facilities like the TCC2 and TDC2 to ensure SPS operation and safety of personnel, by providing more accurate seismic analysis.*

1. Introduction

The structural design standards bind the assessment and verification of the dynamic stability of the load-bearing elements of a building or industrial infrastructure to the seismic hazard of a certain site. The validity of the design largely depends on level of representativeness of the seismic hazard curves and, more precisely, on the local representativeness of the damping profiles of the ground motion variables estimated using the data recorded by a seismic monitoring accelerometer station network. The accuracy of the local estimate depends on the ratio between the number of information collected and the amount of information necessary to describe, with a given accuracy, the phenomenon of propagation of seismic motion in rock formations. Consequently, a first step to reduce the overall uncertainty of the estimate is the availability of a seismic monitoring network coupled with the information that takes into account the position of active faults capable of generating earthquakes, the geomorphological characteristics of rocks and the lithological features of the ground (Capello et al., 1987).

However, at the same time, it is necessary to develop and validate an efficient numerical estimation methodology that allows to exploit all information included in the seismic data and to model the spatial oriented variations between and among the same data, by the so called Spatial Oriented Variography. It is to pursue this objective that, starting from the scientific works of Campbell (1985; 2003), Boor et al. (1994), Sabetta and Pugliese (1996) Hernandez et al. (2004) and Irwansyah et al. (2013), the non-stationary geostatistical estimator was tested to estimate and validate the PGA numerical values and arrival time at the nodes of a predefined grid around the epicentral zones of the earthquakes that occurred in Italy in 2016 (Guarascio et al., 2022).

In this paper the same non-stationary geostatistical model has been used to estimate the PGA components (North-South, and vertical) and the related arrival time of the earthquake which occurred approximately 30 km South-West of the CERN area on 1st November 2022, having Local Magnitude (ML) of 3.4. The estimation values of the PGA at the nodes of 1 km space grid were used to determine the directional damping profiles of the seismic motion with the epicentral directional distances. Finally, the seismic hazard curve was drawn at a point in proximity of the TDC2/TCC2 facility for seismic events located in the area in the azimuthal sector of greatest seismicity around the CERN area that is the 135° azimuth sector South-West to East.

2. Seismicity of the territory around CERN

To assess the seismicity of the territory in the surrounding of CERN, earthquake lists from the past 323 years within a 150-km radius were obtained from the websites of the national geophysical services of Switzerland, France, and Italy. For each earthquake, the geographical coordinates of the epicentre and the intensity, expressed either in European Macroseismic Scale (EMS) or Richter Magnitude scale, were collected. The empirical relationships proposed by Camassi and Stucchi (1997) and Gomez et al. (2019) were used to estimate the epicentral peak ground acceleration (PGA) from the earthquake EMS intensity and Richter magnitude values. Below the intensity of seismic events is expressed by the epicentral PGA. The geographical distribution of earthquakes in the mentioned area is not uniform. The majority of earthquakes and events with the highest epicentral intensity (PGA > 400 cm/sec^2) are predominantly located to the South and South-East of CERN facilities. Of particular note is the earthquake that occurred in 1822 to the North of Lake Le Bourget, roughly 50 km southwest of Geneva (Chapron et al., 1999). This earthquake was estimated to have a magnitude between VII and VIII on the Richter scale, corresponding to an epicentral PGA of approximately 800 cm/sec^2. The Le Bourget earthquake aligns to the North with an event from 1971 with an epicentral PGA of approximately 600 cm/sec^2, and to the North-East with five events of the same intensity that occurred in the sequence of 1839, 1877, 1879, 1936, and 1968. Figure 1 shows the positions of these earthquakes, having a PGA greater than 400 cm/sec^2 with a distance less than 65 km from the TDC2/TCC2 facility. Table 1 shows the number of earthquakes that occurred over the past 323 years within the 8 circular sectors of 45° width, where ° indicates sexagesimal degrees, and centred in the TDC2/TCC2 facility; the events are categorized by their epicentral PGA. For some PGA ranges, it was calculated the parameter λ of the Poisson distribution function, representing the probability of occurrence for a seismic event within that range in a given year. The inverse of the parameter λ provides an estimate of the average time interval between two seismic events having a PGA in the same range.

From the data presented in Table 1, the seismicity of the mentioned 8 circular sectors was estimated (Figure 1). The measurement of the seismicity of this territory is defined as the probability of occurrence of seismic events; this level of seismicity can also be expressed as the average return period of seismic events with epicentral PGA greater than certain intensity thresholds.

3. Universal CoKriging geostatistical estimator of the seismic variables

3.1. Preliminary considerations

A first spatial trend of the damping of the seismic variables' (peak displacement, velocity and acceleration) with the distance from the epicentral zone is obtained from the physical theory of propagation of elastic waves, radially emitted by a point source in a homogeneous and isotropic material. The theoretical result shows a damping law of elastic oscillations (geometric attenuation), inversely proportional with the distance from the source that can be described by the Equation $f(r) = a\, r^{c}$, where $f(\cdot)$ is a function of the distance r of a generic point from the epicentre providing the generic seismic variable (i.e., peak displacement, velocity or acceleration) and a is a constant depending on the seismic variable of interest. The exponent c is equal to 1 for volume waves while is equal to 0.5 for surface ones.

The values recorded by the accelerometer stations deviate from the values predicted by physical theory due to the heterogeneity and discontinuity of the rock formations crossed by seismic waves. Indeed, the different propagation speeds of the seismic waves in the rock formations deform the geometry of the surface waves with consequent irregular and anisotropic variations of the geometric attenuation; furthermore, irregular local variations of the seismic motions are a consequence of the different anelastic behavior of the rock formations. A part of the energy carried by seismic waves is continuously and irregularly dissipated by friction in an anelastic damping mechanism.

Despite this, the data recorded over distances of tens of kilometres from the epicentral zone by the accelerometer stations show good consistency with the mentioned surface wave attenuation equation and the motion anelastic dissipation, which follows an exponential law from the epicentre such as $e^{-b\, r}$, where b is a constant depending on the rock damping properties. The accelerograms recorded by the stations of the seismic monitoring network represent a spatio-temporal sampling of the phenomenon of propagation of the ground seismic motion in the neighbourhood of the epicentral zone for a certain earthquake.

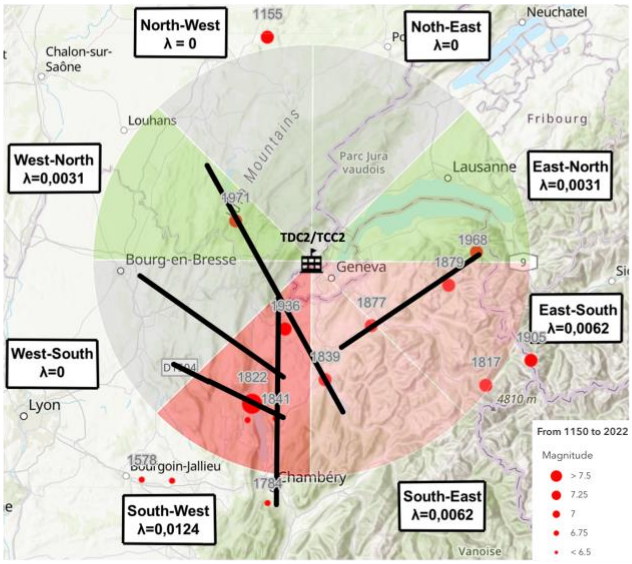

Figure 1. The map illustrates the fault lines associated with the most intense earthquakes (PGA ≥ 400 cm/sec²) and the 8 circular sectors centred in the TDC2/TCC2 facility. The parameter λ of the Poisson distribution represents the ratio between the number of earthquakes with PGA≥400 cm/sec² and the observation period (323 years).

Table 1. Number of detected earthquakes around TDC2/TCC2 facility in the last 323 years, used for the Hazard Rate (λ) estimation and the corresponding Return Period (1/λ) of future seismic events in the 8 circular sectors investigated.

Range of estimated epicentral accelerations (cm/sec^2)	Num. years	East-North		North-East		North-West		West-North		West-South		South-West		South-East		East-South	
		Num. Events (*)	Return period (years)	Num. Events (*)	Return period (years)	Num. Events (*)	Return period (years)	Num. Events (*)	Return period (years)	Num. Events (*)	Return period (years)	Num. Events (*)	Return period (years)	Num. Events (*)	Return period (years)	Num. Events (*)	Return period (years)
5 ≤ PGA < 30	47	35	1.34	12.00	3.92	8	5.88	4	11.75	6	7.83	13	3.62	34	1.38	26	1.81
30 ≤ PGA < 60	147	3	49.00	1	147.00	0		0		0		4	36.75	6	24.50	2	73.50
60 ≤ PGA < 100	323	2	161.50	1	323.00	2	161.50	0		0		3	107.67	4	80.75	2	161.50
100 ≤ PGA < 200	323	1	323.00	0		2	161.50	1	323.00	1	323.00	11	29.36	3	107.67	6	53.83
200 ≤ PGA < 400	323	0		0		0		0		0		1	323.00	0		1	323.00
400 ≤ PGA < 600	323	1	323.00	0		0		1	323.00	0		3	107.67	2	161.50	2	161.50
PGA ≥ 600	323	0		0		0		0		0		1	323.00	0		0	
Total events		**42**		**14**		**12**		**6**		**7**		**36**		**49**		**39**	

(*) Earthquakes with a maximum distance from CERN of 65 km

3.2. Definition of the geostatistical estimator for the seismic variables

The geostatistical estimator is defined as an application of random functions of variables defined on a certain Euclidean space of a rock-like medium (Chilés and Delfiner, 2012; Guarascio, 1976a; Delfiner, 1976). For our purposes, it was chosen the Universal CoKriging (UCoK) with external drift as it allows to integrate: i) the physical law of damping of anelastic waves, which we call in the following the Seismic First-Guess (SFG); ii) the morphology of the topographic surface; iii) the position of the relevant accelerometer stations and iv) the geographical continuity of the seismic variables, which can be described by a variogram and a cross-variogram model (Matheron, 1971).

Let $Z=\{Z(\mathbf{x}): \mathbf{x} \in D \subseteq \mathbb{R}^2\}$, where $\mathbf{x}$ is the 2-dimensional coordinate vector of a generic point, be a non-stationary random field defined on the investigated continuous domain D of the Euclidean space $\mathbb{R}^2$ and reflecting the defining seismic variable at the altitude of the earth's surface (seismic ground motions). We consider then the random function of Z as described by the following Equation:

$$Z(\mathbf{x}) = m(\mathbf{x})+\sigma(\mathbf{x})Y(\mathbf{x}), \quad \forall\ \mathbf{x}\in D \tag{1}$$

where $m(\mathbf{x}) : \mathbb{R}^2 \rightarrow \mathbb{R}$ is the SFG function describing the geographic pattern of the seismic variable on the topographic surface, $\sigma(\mathbf{x}) : \mathbb{R}^2 \rightarrow \mathbb{R}^+$ is the standard deviation of the punctual local variability for the residual from $m(\mathbf{x})$, and $Y(\mathbf{x})$ is a quasi-stationary random field with zero-mean and variogram function $\gamma(\mathbf{h})$, where $\mathbf{h}$ is the origin free distance vector operator (Guarascio et al., 1976b), as defined by Chilés and Delfiner (2012).

The UcoK estimator was used to calculate the value and the arrival time of the PGA by setting the respective SFG of each of these seismic variables. Indeed, the UcoK estimator is herein considered as an estimation $Z^*(\mathbf{x})$ at a point of coordinates $\mathbf{x}$ of the seismic variable Z, which can be either the PGA value or the related arrival time. It can be obtained as a linear combination of the data Z_0 of the variable to be estimated and the data Z_1 of the auxiliary variable around the point of interest:

$$Z_0^*(\mathbf{x})=\sum_{k=0}^{1}\sum_{i=1}^{n}\lambda_{k,i}Z_k(\mathbf{x}_i) \tag{2}$$

where $\lambda_{0,i}$ are the weighting coefficients of the variable Z_0 to be estimated.

3.3. SFG equation for the seismic variables

SFG equation for both PGA values and the related arrival time are herein presented.

The systematic decrease of PGA with distance from the epicentral zone was modelled as a product of the mentioned geometric attenuation of the PGA and the anelastic dissipation laws. The effect of the earth's surface morphology on the seismic ground motion is also modelled. The SFG for the PGA is herein indicated as m_{PGA} and can be defined as:

$$m_{\mathrm{PGA}}(\mathbf{x})= c_{0,\mathrm{PGA}}+c_{1,\mathrm{PGA}}q(\mathbf{x})+c_{2,\mathrm{PGA}}\frac{1}{\sqrt{\bar{d}_s(\mathbf{x},\mathbf{x}_0)}}e^{-b\,\bar{d}_s(\mathbf{x},\mathbf{x}_0)} \tag{3}$$

where $\mathbf{x}_0$ identifies the coordinates of the centre of the earthquake epicentral zone (circle of radius 3.5 km), $q(\mathbf{x}) : \mathbb{R}^2 \rightarrow \mathbb{R}$ is its elevation on the earth surface, $\bar{d}_s(\mathbf{x},\mathbf{x}_0) : \mathbb{R}^2 \rightarrow \mathbb{R}^+$ is the directional anisotropic proximity distance of the point $\mathbf{x}$ from the epicentral zone centred at the point $\mathbf{x}_0$ (non-Euclidean mean distance), b is the coefficient of the anelastic dissipation law and $c_{0,\mathrm{PGA}}$, $c_{1,\mathrm{PGA}}$ and $c_{2,\mathrm{PGA}}$ are three real coefficients.

The SFG for the PGA arrival time m_t increases with distance from the epicentral zone and the related equation is defined in a similar way, such as:

$$m_t(\mathbf{x})=c_{0,t}+c_{1,t}q(\mathbf{x})+c_{2,t}\bar{d}_s(\mathbf{x},\mathbf{x}_0), \tag{4}$$

with akin meaning of the symbols used in Equation (3).

4. Seismic survey of the earthquake event of 1st November 2022

The accelerograms recorded by 58 accelerometer stations during the earthquake on 1st November 2022 (epicentral zone about 30 km South-West from CERN) were processed to determine the directional attenuation profiles of the seismic motion in the rock formations around the CERN area. This seismic event was chosen because it is the most recent earthquake near the CERN area with the greatest intensity since the previous significant event occurred in Frangy on 29th May 1975, which consisted of a shallow main shock followed by two aftershocks (Thouvenot et al., 1998). The seismic variables (PGA value and arrival time) around 60 km from the TDC2/TCC2 facility were estimated at the nodes of a 1 km space grid using the recorded data from the 56 surface accelerometer stations belonging to the seismic monitoring networks of Switzerland, France and Italy.

4.1. SFG equation of the seismic variables

The maximum 3D-oscillation component PGAs during the earthquake of 1st November 2022 were recorded by the station with the code SAVIG. This station was found to be the closest to the epicentre of this seismic event. The oscillation component PGAs recorded by this station are 3.474 cm/sec² in the North-South direction (PGA_{NS}), 3.224 cm/sec² in the East-West direction (PGA_{EW}) and 1.541 cm/sec² vertically (PGA_{Vert}) (Table 2). In particular, the CERNS station, located at 23 km North of the SAVIG station, recorded the following oscillation component PGAs: 0.865 cm/sec² in the North-South direction, 0.690 cm/sec² in the East-West direction and 0.413 cm/sec² vertically. Further considerations on the interpretation of the data recorded by the CERN underground and surface accelerometer stations are presented in the Annex I of this paper.

Table 2. Percentiles of the oscillation component PGAs in the North-South, East-West and Vertical directions recorded in the 58 station points during the earthquake of 1st November 2022.

Seismic variable	Number of station points	25-th percentile	50-th percentile	90-th percentile	Maximum value
$PGA_{N\text{-}S}$	58	0.0818	0.1928	0.7848	3.4736
$PGA_{E\text{-}W}$	58	0.0799	0.2169	0.7686	3.2243
PGA_{Vert}	58	0.0609	0.1609	0.5661	1.5410

The scatter plot in Figure 2 shows the damping in function of the distance from the epicentral zone for the PGA_{NS} values recorded at the station points. This graph shows a lower attenuation of the PGA_{NS} at the station points located in the East-West side with an angular tolerance of ±25° compared to the station points located on the North-South side with the same tolerance of ±25°. This anisotropic damping of the seismic ground motion between the 2 geographical directions is detectable only for distances greater than 60 km. The same damping anisotropy was detected on the two components PGA_{EW} and PGA_{Vert}.

The coordinates of the centre of the epicentral zone and the coefficients of the SFG, Equation (3), for the PGA_{NS} and PGA_{Vert} were calculated using Markov Chain Monte Carlo (MCMC) simulations to solve the following minimization problem:

$$\mathbf{C}(\mathbf{x})=\min_{\boldsymbol{\theta}(\mathbf{x})\in\Theta}\left\{\sum\left[z_{\mathrm{PGA}}(\mathbf{x}_i)-m_{\mathrm{PGA}}(\mathbf{x}_i)\right]^2\right\} \tag{5}$$

where $z_{\mathrm{PGA}}(\mathbf{x}_i)$ stands for the PGA value recorded in the station having coordinates $\mathbf{x}_i$, $\boldsymbol{\theta}(\mathbf{x})$ is the 2-component vector consisting of the anelastic damping parameter and the diagonal elements of the metric tensor matrix normalized to the value for the North-South geographical direction, and $\mathbf{C}(\mathbf{x})$ is the vector of the coefficients of the related SFG equations. Both vectors were referenced to the grid nodes' coordinates.

In particular, for each grid node, samples of N pairs of values for the anelastic damping parameter and of the diagonal elements of metric tensor matrix were randomly generated within a predefined range of variation. These sample pairs describe the seismic damping law around each grid node. Each sample pairs differ from the previously generated one for a small random variation. The sample pair values are accepted or rejected in the MCMC process on the basis of the Root Mean Squared Error (RMSE) calculated on the recorded data at the station points. The epicentral zone is centred on the grid node with the lowest RMSE. The SFG equations of for the seismic variables are calculated for this grid node as well. The coefficients of the two SFG equations are estimated by linear regressions using the observed data at the station points (Figure 2).

4.2. Cross-Validation of the UCoK unbiased estimator

UcoK estimator at any station point where the seismic variable has to be estimated is given as a weighted average of the data of the PGA values and the PGA arrival times at those station points located in the related neighbourhood. The estimation of the weighting coefficients in Equation (2) and the variance of the estimation error of each seismic variable depend on the local variability of the ground motion; this is maximum near the epicentral zone of the earthquake and decreases with distance. For this reason, the variogram $\gamma_{PGA}(\mathbf{h})$, was calculated as the average of the squared differences of the normalized residuals $y'_{PGA}(\mathbf{x}) = [y_{PGA}(\mathbf{x}) - m_{PGA}(\mathbf{x})]/\sigma(\mathbf{x})$; the $\gamma_{PGA}(\mathbf{h})$ is calculated as the difference between the pairs of station points grouped by distance and direction classes (Chilés and Delfiner, 2012). The local variance of the residuals $\sigma(\mathbf{x})$ was expressed as a function of $m(\mathbf{x})$. In geostatistics, the functional relationship between $\sigma(\mathbf{x})$ and $m(\mathbf{x})$ is defined as a proportional effect (Chilés and Delfiner, 2012). The PGA normalized residuals were used also to calculate the cross-variogram between PGA values and PGA arrival time.

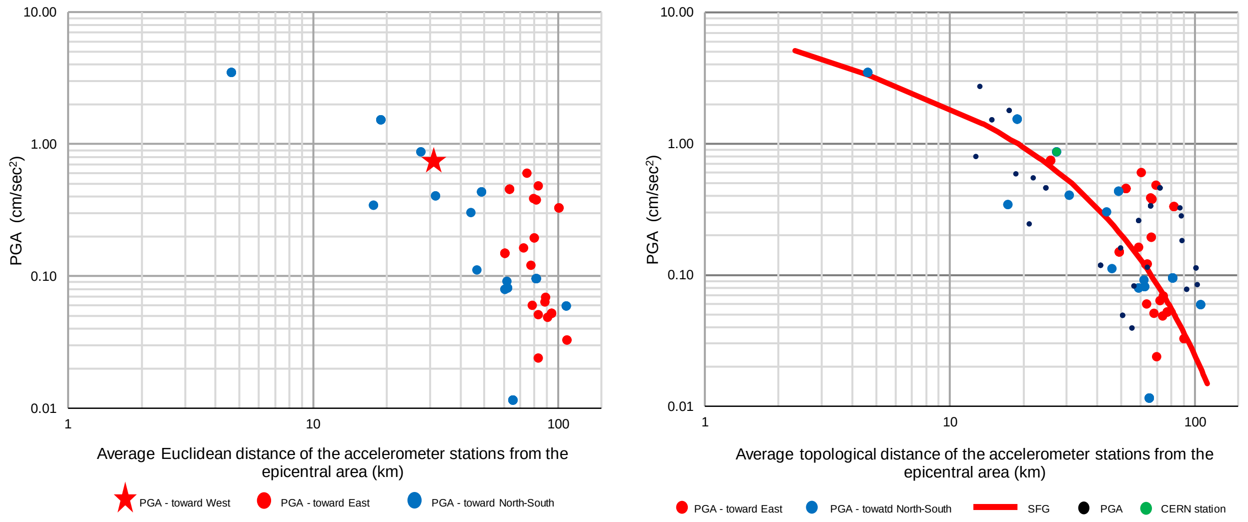

Figure 2. Earthquake of 1st Nov. 2022 (ML=3.4) – North-South component PGA. In the graph on the left is the scatter-diagram of the PGA at the station points in the East-West direction (red dots) around epicentral zone that are mainly arranged in the upper part of the point cloud. In the East-West direction, the accelerometer stations located East of the epicentral area (±25° East) have a distance greater than 60 km, while only one station is located West of the epicentral area (red star); in the graph on the right is the same scatter-diagram with the seismic proximity distance on the horizontal axis.

Once the coefficients of the SFG equations have been calculated and the variograms and cross-variogram of the seismic variables have been modelled, the whole estimation process for all grid nodes can be implemented as a sequence of numerical calculations well tested in practice. The cross-validation phase of the chosen estimator is carried out for the purpose of verifying the representativeness of the variogram and cross-variogram models on the available data (Matheron, 1989). The UCoK estimator with external drift was applied to estimate the seismic variables at all station points, without considering the data in the station point where the variables are estimated. This way the following information is available for the 56 station points: i) the recorded data during the seismic event; ii) the UCoK estimations; iii) the committed estimation error, calculated as the difference between estimated value and recorded data; and iv) the variance of the estimation error calculated by the UCoK estimator.

From the cross-validation results it is revealed that for the two seismic variables: i) the average of the estimation errors at the station points is close to zero and ii) the dispersion variance of the same estimation errors is close to the average value of the estimation variances predicted by the UCoK estimator in the station points (Table 3). Figure 3 compares the estimated PGA values with the PGA recorded from the 56 station points.

Table 3. Statistical parameters of the seismic variables calculated on the recorded data, on the estimate errors and on the estimate variances predicted by the UCoK estimator.

Seismic variable	Number of station points	Data Average	Data Minimum	Data Maximum	Average error	Variance error	CoKriging Variance
PGA_{N-S}	56	0.4219	0.0115	3.4736	0.0195	0.1197	0.1199
PGA_{N-S} Arrival Time	56	82.78	64.1	109.22	0.08	19.87	19.47

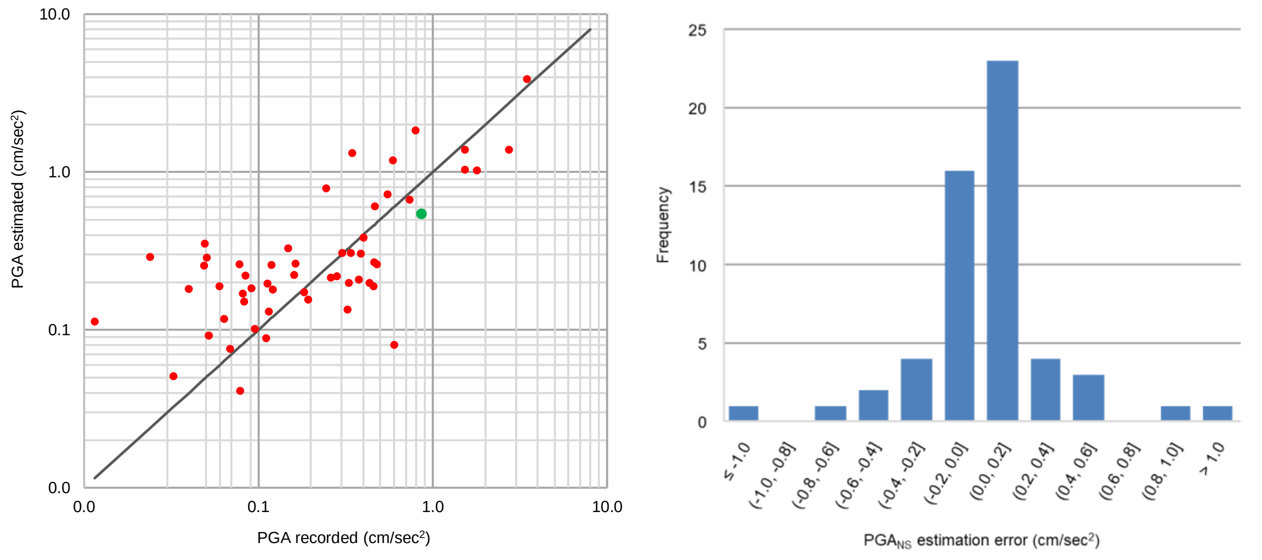

Figure 3. Earthquake of 1st Nov. 2022 (ML=3.4) – North-South component PGA. In the graph on the left is the scatter-diagram of the estimated PGA_{NS} values at the station points versus the data recorded by the accelerometer stations. The green dot represents the PGA_{NS} estimated at the location point of the CERNS station. The graph on the right shows the histogram of the PGA_{NS} estimation errors in the 56 station points, from which it is visible how the UCoK estimator be unbiased as the error distribution mean tends to zero and the shape is symmetrical.

4.3. Damping PGA profiles' modelling

The seismic variables of the ground motion were reconstructed around the epicentral area of the earthquake of 1st November 2022. The PGA values and the respective arrival time of the two oscillation components were estimated at the nodes of a 1 km space grid using the UCoK estimator.

A dynamic search algorithm was used to select the stations in the estimation neighbourhood of each grid node. Such an algorithm selects the two closest stations for each of the 8 circular sectors of 45° angular width and centred in the node to be estimated. If there is no data in more contiguous circular sectors, the algorithm increases the data of the other circular sectors, searching the nearest station to the first selected pair of stations. A grid node is not estimated if it does not have at least 6 stations in the node neighbourhood. Figure 4 shows the PGA_{NS} map around the epicentral zone of the earthquake of 1st November 2022.

The estimated PGA at the grid nodes were used to plot the directional PGA damping profiles in function of the epicentral distance towards the East (0° East), North (90° East), West (180° East) and South (270° East). The directional damping profiles were discretized into 2.5 km steps and the PGA value assigned to each step was calculated as the arithmetic means of the PGA values of the grid nodes inside the circular crowns having 2.5 km length and angular width ± 22.5° with respect to the profile direction (Figure 4).

5. Seismic hazard curve at the location of the TDC2/TCC2 facility

As mentioned, the level of seismicity of the territory is not uniform in the various sectors around the CERN area. The probability of occurrence of earthquakes with an epicentral PGA greater than 100 cm/sec^2 in the South to East sector (approximately 5000 km^2) is 4.3 time higher than the probability of occurrence of earthquakes of the same intensity level located in the Northern zone from East to South-West of the CERN area (8200 km^2). This result has suggested to concentrate our investigation for modelling the corresponding seismic hazard curve to the 135° circular sector between South-West and East directions (Figure 1). Consequently, the probabilities that future seismic events in this area could generate a ground acceleration at the TDC2/TCC2 facility greater than 5 cm/sec^2 have been reported on the seismic hazard curve, plotted on the basis of the seismicity of the area observed over the last 323 years, in conjunction with the PGA damping model of 1st November 2022 earthquake.

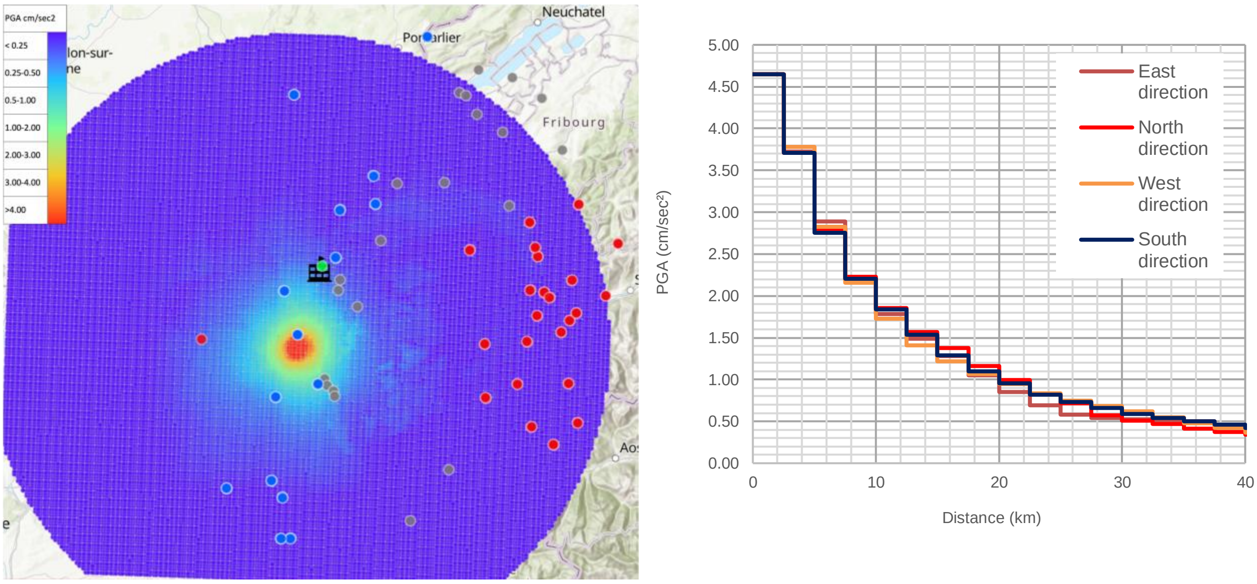

Figure 4. The map on the left represents the areal damping pattern of the PGA North-South component of the 1st November 2022 earthquake reconstructed at the nodes of a 1-km space grid. The estimated values of the PGA at the grid nodes is everywhere consistent with the physical theory of propagation of the oscillatory movement in a homogeneous medium with radial anisotropy, as described by the SFG. Locally, the seismic data recorded at the station points, containing information on the lithological heterogeneity of the rocks, return a PGA value more consistent with the local lithological and mechanical characteristics of the subsoil (seismic micromodelling zoning). The UCoK estimator made it possible to integrate the physical damping law of seismic motion and the sampled seismic data, returning a spatial model of the PGA. The PGA values given by such a spatial model are consistent with a rock model whose lithological characteristics are a spatial average of those related to the real rock volumes crossed from seismic waves, that converge to the most representative values where the data are present. These are the zones in which the variance of the estimation error is lower. The graph on the right shows the PGA damping profiles of the PGA North-South oscillation component, according to the four main propagation directions, in function of the epicentral distance, for each geographical direction.

In particular, the probability that the target point can perceive a PGA greater than a threshold value (PGA_k) is proportional to the extension of the area of the circular crowns, in which any earthquake generates a ground acceleration greater than PGA_k at the target point. In other terms, the probability that an earthquake of a seismic intensity E_i, for the *i*-range introduced in Table 1, falls within the circular crowns whose damped ground acceleration peaks are greater than PGA_k (Figure 5a) is given by:

$$P_i(\mathrm{PGA}_k)= \frac{a_i(\mathrm{PGA}_k)}{\mathrm{A}} \; P(E_i) \tag{6}$$

Where $a_i(PGA_k)$ is the area of the circular crowns with damped ground acceleration greater than PGA_k generated by a seismic event of intensity in the range E_i, A is the area of the South-West to East sector (5000 km^2) and $P(E_i)$ is the probability that one or more seismic events of intensity in the range E_i occur in the area A in a year: $P(E_i)=1/T_{rp},(E_i)$, where $T_{rp}(E_i)$ is the return period of seismic events of intensity in the range E_i.

The damping profiles of the PGA in the North direction for the events belonging to the 7 seismic intensity ranges were drawn up by rescaling them to the lower bound of the seismic intensity ranges (Table 1) at the first step of the PGA damping profile of the seismic event of 1st November 2022 (epicentral PGA equal to 4.7 cm/sec^2).

The variances of the estimation error of the PGA values at the grid nodes, predicted by the UCoK estimator, were used to calculate the variation range of the PGA damping profiles. The seismic hazard curves were then drawn by repeating the calculation of $P_i(PGA_k)$ first with the minimum PGA damping profile and then with the maximum one (Figure 5b).

From the seismic hazard curves shown in Figure 5b, the PGA values for return period of 475 years and 975 years have been identified, as they are used in design of structures respectively for the life-safety and collapse limit states (CEN, 2004), which are used to determine seismic actions for design and dynamic stability verification of buildings and infrastructures. Specifically, at the point in correspondence of TDC2/TCC2 facility, the PGA values for return periods of 475 years and 975 years are respectively 185 cm/sec^2 (confidence range from 113 to 224 cm/sec^2) and 248 cm/sec^2 (confidence range from 203 to 313 cm/sec^2), respectively.

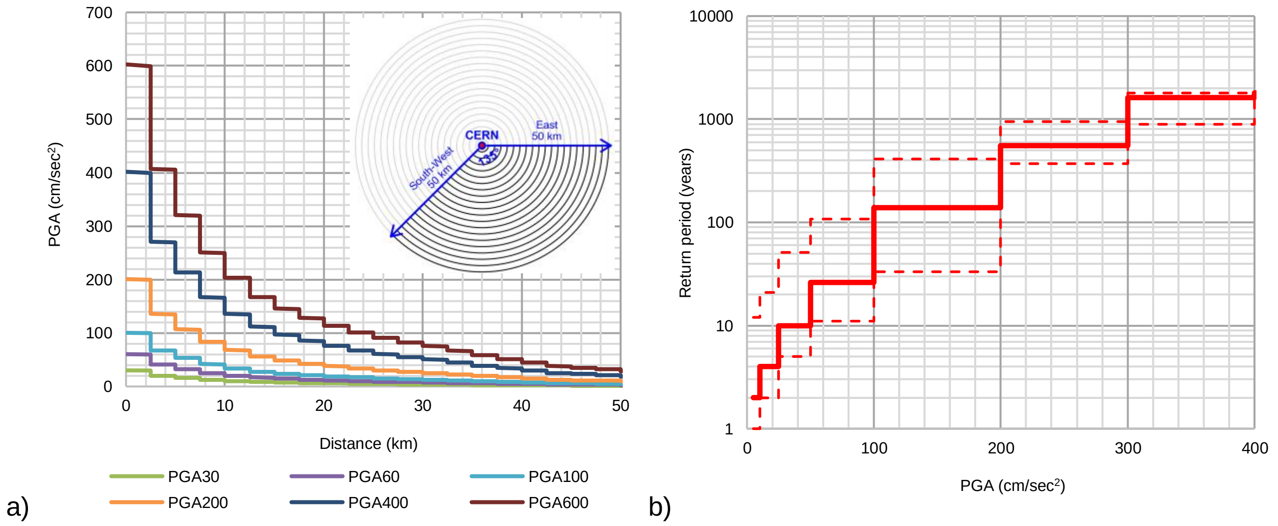

Figure 5. a) PGA Damping Profiles Models for the North-South oscillation component in function of the epicentral distance. The Models are staircase-type curves where the runs of each step describe circular crowns of 2.5 km width at various distances from the centre (CERN point). In the vertical axis are the values of PGA in the epicentral area, ranged from 30 to 600 cm/sec^2. b) Seismic hazard curve at the TDC2/TCC2 facility for earthquakes in the South-West to East sector. The graph also shows the range of variation due to the PGA estimation error.

6. Conclusion

The study highlights how the use of geostatistical estimated seismic variables at grid points does properly and effectively represent the seismic phenomena, across the entire geographical domain, considering the use for engineering purposes, namely the damping and point hazard curve characterization. The local information data lack is compensated by assuming the SFG as a physical model representing elastic and anelastic damping in the rocks. Such a compensation is also quantified in the modelling of the related variogram and the cross-variogram. The variogram and cross-variogram models characterize the type of geographical continuity of the seismic variables presented herein in 2-dimensions and then adding a third dimension by considering the PGA arrival time also. The observed data have supported the identification of a physical model and representativeness of the variograms and cross-variogram models for taking into account the geological conditions including discontinuities, heterogeneities and anisotropies.

The UCoK estimator has been applied taking advantage from the recorded data by the seismic stations around each node of a 1 km space grid providing, together with the seismic variable estimated values, the indicator of accuracy of the estimation itself (UCoK standard deviation of the estimation errors). The above estimated values have been cross-validated at the point of the accelerometric stations where both the recorded data and estimated ones are available. The results of the above cross-validation procedure have been reasonably satisfactory and then the presented seismic hazard curve obtained at the point in correspondence of CERN TDC2/TCC2 facility can be considered with a high level of confidence.

As a future development, the use of the data recorded in the underground stations of CERN will permit to have a better understanding of the phenomena tied to the wall wave propagation in the CERN Large Hadron Collider (LHC) circular tunnel. Indeed, the accelerograms recorded in such underground stations show an increase of the acceleration in proximity of the points farer from the epicentral zone. Some hints are anticipated in the Annex I of this paper.

7. References

Camassi R., & Stucchi M. (1997). NT4. 1 un catalogo parametrico di terremoti di area italiana al di sopra della soglia del danno. Consiglio Nazionale delle Richerche, Gruppo Nazionale per la Difesa dai Terremoti.

Campbell K. W. (1985). Strong Motion Attenuation Relations: A Ten-Year Perspective. Earthquake Spectra, 1(4), 759-804. https://doi.org/10.1193/1.1585292.

Campbell K. W. (2003). Prediction of Strong Ground Motion Using the Hybrid Empirical Method and Its Use in the Development of Ground-Motion Relations in Eastern North America - Bulletin of the Seismological Society of America, vol 93, no 3, (pp. 1012–1033). https://doi.org/10.1785/0120020002

Capello G., Guarascio M., Libertà A., Salvato L., Sanna G. (1987). Multipurpose Geostatistical Modelling of a Bauxite Orebody in Sardinia. In: Matheron G., Armstrong M. (eds) Geostatistical Case Studies. Quantitative Geology and Geostatistics, vol 2. Springer, Dordrecht.

CEN (2004). EN 1998-1:2004. Eurocode 8: Design of structures for earthquake resistance - Part 1: general rules, seismic actions and rules for buildings. European Committee for Standardisation (CEN), Bruxelles, Belgium.

Chapron E., Beck C., Pourchet M., & Deconinck J. F. (1999). 1822 earthquake-triggered homogenite in Lake Le Bourget (NW Alps). Terra Nova, 11(2-3), 86-92. https://doi.org/10.1046/j.1365-3121.1999.00230.x.

Chiles J. P., & Delfiner P. (2012). Geostatistics: Modeling Spatial Uncertainty (Second Edition). John Wiley & Sons. https://doi.org/10.1002/9781118136188

Delfiner P. (1976). Linear Estimation of non Stationary Spatial Phenomena. In: Guarascio M., David M., Huijbregts C. (eds) Advanced Geostatistics in the Mining Industry. NATO Advanced Study Institutes Series, vol 24. (pp. 49-68). Springer, Dordrecht. https://doi.org/10.1007/978-94-010-1470-0_4

Gomez Capera. A. A., Santulin M., Massa M., Locati L., Puglia R. (2019). Conversione tra parametri del moto del suolo e intensità macrosismica. CPS-INGV.

Guarascio M. (1976b). Improving the Uranium Deposits Estimations (The Novazza Case). In M. Guarascio, M. David, & C. Huijbregts (eds.), Advanced Geostatistics in the Mining Industry. NATO Advanced Study Institutes Series, vol 24. (pp. 351-367). Springer. Dordrecht.

Guarascio M. (1979). Optimization of sampling patterns and of block estimation methods. In Evaluation of uranium resources. (pp. 145 – 175). IAEA. Vienna.

Guarascio M., Huybrechts C. J., David M. (1976a). Advanced Geostatistics in the Mining Industry. Proceedings of the NATO Advanced Study Institute held at the Istituto di Geologia Applicata of the University of Rome, Italy, 13–25 October. https://doi.org/10.1007/978-94-010-1470-0

Guarascio M., Libertà A., Berardi D., Alakbarli E., & Lombardi M. (2022). Geostatistical modeling of seismic actions on the structural components of the San Benedetto Road tunnel, Italy. Risk Analysis, Hazard Mitigation and Safety and Security Engineering XIII, 214, 27. https://doi.org/10.2495/SSR220021

Hernandez B., Cocco M., Cotton F., Stramondo S., Scotti O., Courboulex F., Campillo M. (2004). Rupture history of the 1997 Umbria-Marche (Central Italy) main shocks from the inversion of GPS, DInSAR and near field strong motion data. Ann. Geophys. 47(4). https://doi.org/10.4401/ag-3349.

Matheron G. (1971). The theory of regionalized variables and its applications. – Les cahiers du CMM de Fontainebleau, Fasc. 5, Ecole des Mines de Paris.

Matheron G. (1989). Estimating and Choosing-An Essay on Probability in Practice. Springer, Berlin, Heidelberg. https://doi.org/10.1007/978-3-642-48817-7.

Sabetta F., & Pugliese A. (1996). Estimation of response spectra and simulation of nonstationary earthquake ground motions. Bulletin of the Seismological Society of America, 86(2), 337–352.

Thouvenot F., Fréchet J., Tapponnier P., Thomas J. C., Le Brun B., Ménard G., Lacassin R., Jenatton L., Grasso J.R., Coutant O., Paul A., Hatzfeld D. (1998). The ML 5.3 Epagny (French Alps) earthquake of 1996 July 15: a long-awaited event on the Vuache Fault. Geophysical Journal International, 135(3), 876-892.

Annex I: Further considerations on the interpretation of the data recorded by the CERN underground and surface accelerometer stations

The dynamic ground motion seismic variables in the epicentral zone are quasi-stationary without precise and detectable location definition; the ground motion generate new types of seismic waves, such as the surface waves, which propagate radially only in the most superficial layers of the geostratigraphic system. Out of the epicentral zone, the ground seismic motion is the combination of the vibrational movements related to the surface waves and the vibrational movements related to the volume ones rising from the deeper layers of the geo-stratigraphic configuration. Moving away from the epicentral zone i) the amplitudes of the surface waves become predominant compared to the amplitude of the longitudinal (P) and transversal (S) volume waves, and ii) the ground motion tends to dampen.

The experimental evidence offered by the accelerograms recorded by the 5 surface stations (SAVIG, PERON, CERNS, COLLE and LADOL, as named in the Swiss accelerometer network) and the 2 underground stations of CERN (i.e., CERN1 and CERN5) aligned in the 75° East direction, from SAVIG station (epicentral distance 4.66 km) to LADOL station (epicentral distance 46.62 km), in occasion of the 1st November 2022 earthquake, shows (Figure 6):

- the linear dependence on the distance from the epicentral zone of both the onset time of the ground motion, generated by the volume waves rising from the deeper layers of the geo-stratigraphic configuration (P and S waves), and the PGA arrival time generated by the surface waves (Rayleigh and Love waves);
- the presence of an increase in the acceleration of the seismic motion recorded by the CERN5 underground station about 5 seconds after the arrival time of the volume waves respect to the accelerogram of the CERN1 underground station, which is closest to the epicentral area of about 8.33 km. This second movement is probably generated by the propagation phenomena of wall waves in the LHC tunnel;
- the perfect match of the PGA values recorded by the 5 surface stations with the geometric attenuation law of surface waves, which are inversely proportional to the square root of the distance from the epicentral zone;
- the perfect match of the acceleration peaks in the first second of the seismic motion recorded by the underground stations CERN1 (83.7 m depth) and CERN5 (90.2 m depth) with the geometric attenuation law of volume waves, which appear as inversely proportional to the distance from the hypocentral zone;
- the acceleration peak (0.1193 cm/sec^2) recorded by the CERN1 underground station in the first second of the seismic motion is the maximum of the entire recording. A similar acceleration value (0.1122 cm/sec^2) was recorded by the CERN1 station about 5 seconds after the first peak. On the contrary, the acceleration peaks recorded by the CERNS surface station and the CERN5 underground station are respectively 0.8650 cm/sec^2 and 0.2483 cm/sec^2 and are greater than the accelerations recorded during the first second of the seismic motion, as shown in Table 4. These maximum values of the accelerogram have a delay of about 5 seconds from the acceleration peak recorded during the first second of seismic motion. The order of recording of the above mentioned acceleration peaks suggests that: i) the seismic motion recorded by the CERN1 station can be due only to the volume waves while ii) the acceleration peaks recorded in the other two CERN stations can be attributed to the seismic motion generated by waves, as triggered by volume waves respectively in the surface layer of the geo-stratigraphic configuration and in the rocks around the LHC tunnel.
- the perfect matches between the peak acceleration values recorded by the 3 CERN stations during the first second of the seismic motion and the damping law of the volume waves and between the PGA values recorded by the 5 surface stations and the damping law of the surface waves demonstrate that i) the damping law of the volume waves is not representative of the PGA geographical pattern around the epicentral zone and ii) the PGA values recorded by the surface stations cannot be referred to the deep rock formations (bed-rock).

Further details are expected to be provided in future publications by the authors.

Table 4. Seismic data referred to the stations aligned in the 75° East direction, from SAVIG station (epicentral distance 4.66 km) to LADOL station (epicentral distance 46.62 km), in occasion of the 1st November 2022 earthquake.

Station Code	Elevation	Epicentral distance	Direction	Onset time of the seismic motion	Peak acceleration in first second	Speed between pairs of stations	PGA arrival time	PGA	Speed between pairs of stations	PGA damping compared to epicentral PGA
	(m)	(km)	°East	(sec)	(cm/sec^2)	(km/sec)	(sec)	(cm/sec^2)	(km/sec)	(%)
SAVIG	529	4.6603	89.3	61.93	1.4645		64.105	3.4736		73.91
PERON	708	18.9876	103.7	63.205	0.776	11.24	66.345	1.5262	6.40	32.47
CERNS	463	27.5897	73.00	65.268	0.1539	4.17	69.956	0.865	2.38	18.40
COLLE	447	31.578	66.9	65.96	0.201	5.76	71.215	0.4013	3.17	8.54
LADOL	1455	46.6157	72.8	68.66	0.026	5.57	80.595	0.1105	1.60	2.35
CERN1	356	24.03	73.00	64.70	0.1193		65.376	0.1193		
CERN5	418	32.36	73.00	65.88	0.0873	7.06	71.208	0.2483	1.43	

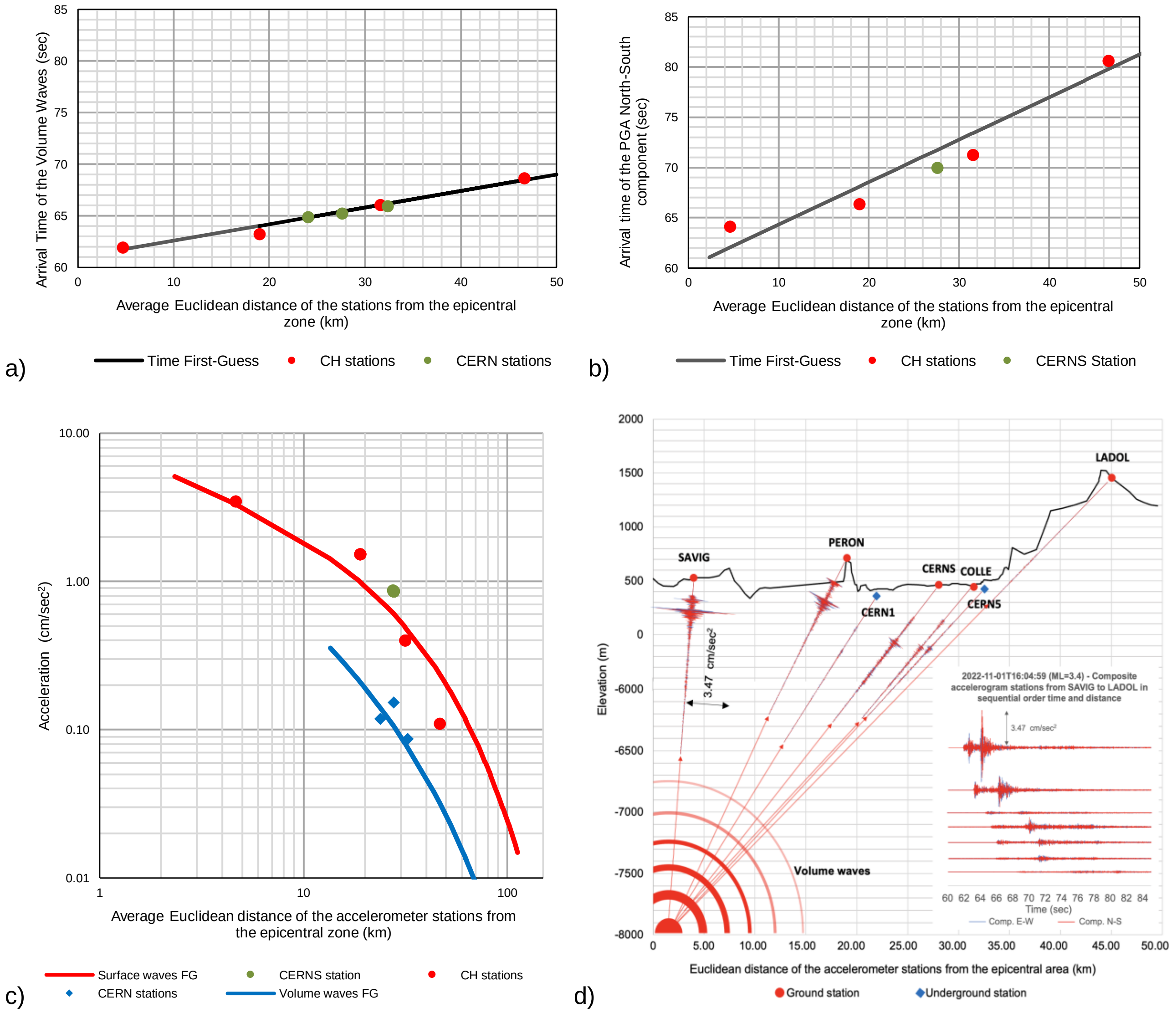

Figure 6. Plots of the seismic data referred to 7 stations aligned in the 75° East direction, from SAVIG to LADOL station, in occasion of the 1st November 2022 earthquake: Function of the distance from the epicentral zone for the a) arrival time of the volume waves, b) arrival time of the PGA North-South component, and c) North-South component of the maximum acceleration of the sole volume waves recorded in the first second in CERN stations (blue) and the PGA recorded in surface stations (red). d) Ground vertical section indicating the recorded accelerograms.